Supporting Information

Adaptable polyionic elastomers with multiple sensations and entropy-driven actuations for prosthetic skins and neuromuscular systems

Zhouyue Lei, [a, b] and Peiyi Wu*[a, b]

[a] State Key Laboratory for Modification of Chemical Fibers and Polymer Materials, College of Chemistry, Chemical Engineering and Biotechnology, Center for Advanced Low-Dimension Materials, Donghua University, Shanghai 201620, China.

[b] State Key Laboratory of Molecular Engineering of Polymers and Department of Macromolecular Science, Fudan University, Shanghai 200433, China.

Corresponding author's email address: wupeiyi@dhu.edu.cn; peiyiwu@fudan.edu.cn

This material includes

Supplementary Movies:

Movie S1. A movie showing the 3D printing process of the polyionic elastomer.

Movie S2. Polyionic skin's sensations towards a plastic hand's movements.

Movie S3. Polyionic skin's sensations towards human finger touch.

Movie S4. Polyionic skin's sensations towards human breath.

Movie S5. Polyionic skin's sensations towards temperature changes.

Movie S6. Polyionic muscle's actuations and real-time sensory feedbacks under the remote NIR stimulus.

Rheological analysis of the 3D printing process

To analyze the rheological behavior of the precursor ink during 3D printing, we measured stress and viscosity as a function of shear rates (Figure 1j). The viscosity shows shear-thinning behavior with η ≈700 Pa s at low shear rates (1 s^{-1}) and η ≈ 35 Pa s at high shear rate (1000 s^{-1}). In this region (1-1000 s^{-1}), a power-law fluid model is applied to describe the shear stress as a function of shear rates, $\tau = K\cdot\dot{\gamma}^{n}$, in which *n* is the exponent and *K* is the consistency index. By performing a power-law fit, the shear-thinning exponent *n* is calculated to be 0.6. When the power-law fluid flowing through a cylindrical tube of radius *r*, the Rabinowitsch–Mooney equation,[1] $\dot{\gamma} = (\frac{3n+1}{4n})\frac{4Q}{\pi r^3}$ in which *Q* is the volumetric flow rate, is utilized to predict the shear rate $\dot{\gamma}$, which is about 12 s^{-1}. Thus, the corresponding viscosity of the ink is about 410 Pa s (Fig. 1a). Immediately after extrusion, the viscosity increases to > 800 Pa s assuming a shear rate of far below 0.1 s^{-1}, and hence allows for shape retention.

Strain sensing analysis

The capacitive strain sensing relays on the mechanism of parallel-plate capacitance, $C = \varepsilon S/4\pi k d$ (*C,* ε, k, *S* and *d*, are the capacitance, dielectric constant of the dielectric layer, electrostatic constant, effective area of the conductive layer, and the thickness of the dielectric layer). Assuming that the device volume and permittivity remain constant,[2] when the device is stretched by a factor, $\lambda = L/L_0$, the area ($S = W L$) of the conductive layer is scaled by a factor of $\sqrt{\lambda}$, and the thickness of the dielectric layer (*d*) is scaled by a factor of $\frac{1}{\sqrt{\lambda}}$. Consequently, the capacitance *C* scales as $C = C_0\lambda$ (C_0 is the initial capacitance) and the strain sensitivity (defined as the change in capacitance induced by strain, i.e., $\frac{d_{\Delta C/C_0}}{d(\lambda-1)}$) is supposed to be a constant of 100% in theory.

Pressure sensing analysis

The capacitive pressure sensing also depends on the dimension change of parallel-plate capacitance. Since the polyionic elastomer has a much higher modulus than the dielectric layer in this case (the compression modulus of the polyionic elastomer and VHB layer is about 470 and 60 kPa, respectively), the capacitance change is mainly owing to the dimension change of dielectric layer. When the device is compressed by a factor of k, the thickness of the dielectric layer is scaled by a factor of 1-k. As a result, the capacitance C scales as $C = C_0 \frac{1}{1-k}$, and the pressure sensitivity is supposed to be related with the modulus (E) of the VHB layer in theory.

Tactile sensing analysis

The tactile sensing mechanism in Figure 3e, f, is owing to the disturbance of the fringing electric field, which is similar to the mechanism used in capacitive touch screens.[3, 4] The capacitance of the sensor includes the plate electrode capacitance and fringing capacitance. In particularly, the 3D printing polyionic grids have larger specific surface area than the bulk materials, and results in more fringing capacitance above the sensor. Different from the strain and pressure sensing capabilities relaying on the dimension changes, when a finger, or to be more general, any of a grounded conducting medium, approaches to the tactile receptor, the fringing electric field (through the medium) is partially intercepted and shunted to ground by the finger and leads to a decrease in capacitance.

As shown in Figure 2e, f, the bare finger produces more decreases of the capacitance upon finger touching (no force applied) owing to higher conductivity of human body without the insulation of the rubber gloves. Nevertheless, the gloved finger can also be detected with measurable capacitance decreases. Therefore, the polyionic elastomer is a promising candidate

for future developments in soft, stretchable and transparent touch panels.[5]

Thermodynamic analysis of the self-powered humidity sensing

Moisture promotes the ionization of one side of the polyionic elastomer, in which more free ions are released, and the gradient distribution of ions enables a diffusion process which can be described as: $J_{dif} = -qD\frac{dc}{dx}$ (J_{dif}, q, D, c and x are diffusion current density, electric quantity of elementary charge, diffusion coefficient, concentration of ions and distance to the surface exposed to moisture, respectively).[6] When the ions migrate and reach the other side, the drift induces electric field between two sides of the polyionic elastomer which can be defined by: $J_{dri} = \sigma E_i$ (J_{dri}, σ and E_i are drift current density, ionic conductivity and induced electric field intensity, respectively). When the thermodynamic equilibrium is established, i.e., $J_{dif} + J_{dri} = 0$, the induced electric field intensity can be described as: $E_i = \frac{qD}{\sigma} \cdot \frac{dc}{dx}$. Therefore, the induced voltage U_i perpendicular to the surface of the polyionic elastomer, can be described as: $U_i = \int \frac{qD}{\sigma} \cdot \frac{dc}{dx}$. Ideally, each part of the polyionic elastomer is supposed to have the same diffusion coefficient and ionic conductivity which are irrelevant with the distance x, and hence the induced voltage U_i can be expressed as: $U_i = \frac{qD}{\sigma} \int \frac{dc}{dx}$, suggesting that the intensity of induced voltage directly corresponds to the gradient of ions.

Temperature sensing analysis

The temperature sensing is based on the resistance–temperature relationship, similar to that found in other types of ionically conductive materials, e.g., ionic liquids[7], ionogels[8] and ionically conductive hydrogels[9]. Moreover, like the previously reported metallo-

supramolecular polymers[10], the polyionic elastomer also displays resistive variations in response to the relative humidity (RH) change. Therefore, we use a hyperplane in the "resistance change vs temperature vs humidity" space to describe the resistive response. The thermo-resistive change is in one to two orders magnitude from 25 to 95 ^{o}C. When the relative conductivity (log(1/R)) was plotted as a function of temperature (1000/T), the polyionic elastomer is observed to follow the simple Arrhenius model.[8] The humidity-induced resistance change is in one order of magnitude from 30% to 90% RH and also exhibits a linear relationship between the log(1/R) and RH. By using an airtight tape (*e.g.*, a VHB tape) to seal the polyionic elastomer, we can thus distinguish the thermal stimulus based on ionic resistance and may choose another bare one to derive the humidity changes via self-powered voltages.

Compared with the previously reported thermal sensors, the sensitivity of the polyionic elastomer is higher than that of gold sensors[11], printable electroconductive temperature sensors (CNT-PEDOT:PSS)[12], self-healing conductive elastomers based on SWCNTs[13], polypyrrole sensors[14], hydrogel sensors,[9] some of electroconductive nanocomposites[15, 16], etc. Although percolation-type thermistors produce a very high $\Delta R/R$ value leading to much higher sensitivity, such resistance changes usually occur in a very narrow temperature range (within 10 °C).[16, 17] In contrast, our platform has a broad temperature sensory range up to 90 ^{o}C in ambient condition (60% RH), wider than that of the gold sensors[11], hydrogel sensors[9] and some of the electroconductive nanocomposites[14, 15]

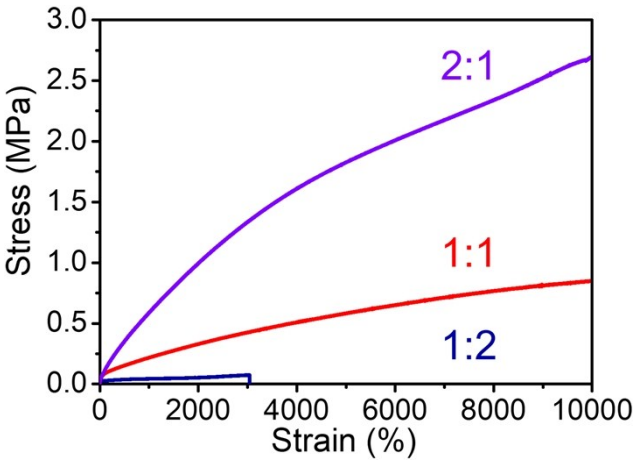

Figure S1. The true tensile stress–strain curves of the polyionic elastomers with different counterion molar ratios. The molar ratio of anionic and cationic units varying from 1:2 to 2:1).

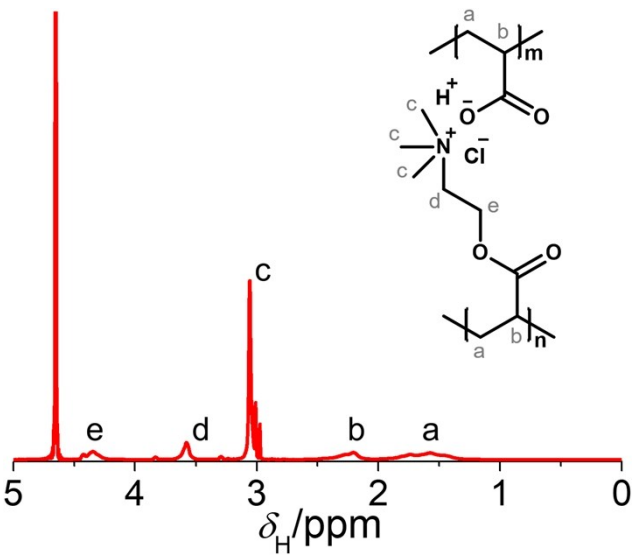

Figure S2. a, ^{1}H-NMR spectrum of the polyionic elastomer. The counterion molar ratio is 1:1.

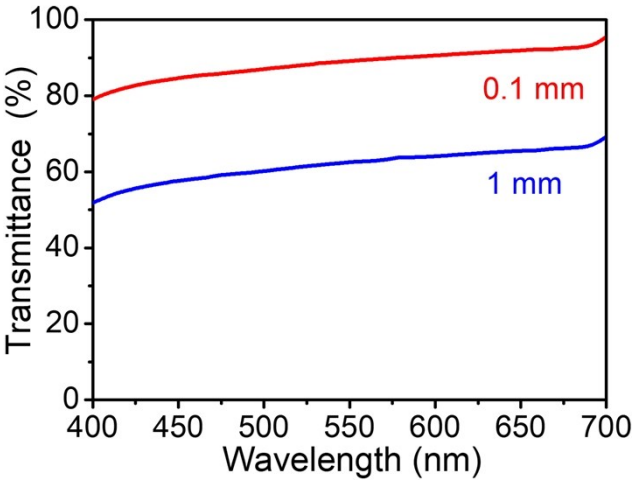

Figure S3. The transmittance of the polyionic elastomers with thicknesses of 1 mm and 0.1 mm in the visible wavelength range of 400-700 nm.

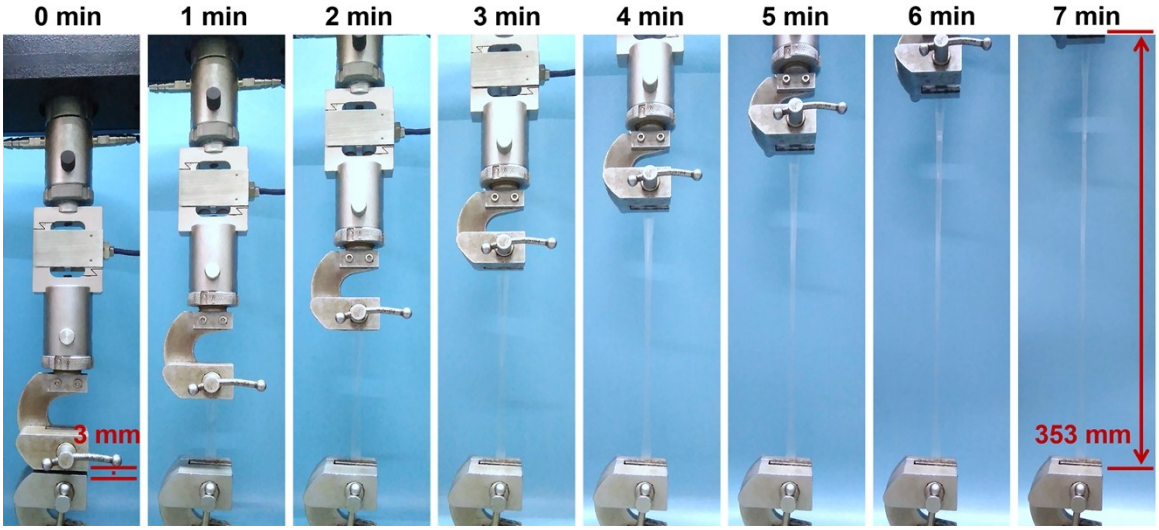

Figure S4. The real-time photographs of the polyionic elastomer which is stretched from an initial length of 3 mm at a deformation rate of 50 mm min^{-1}.

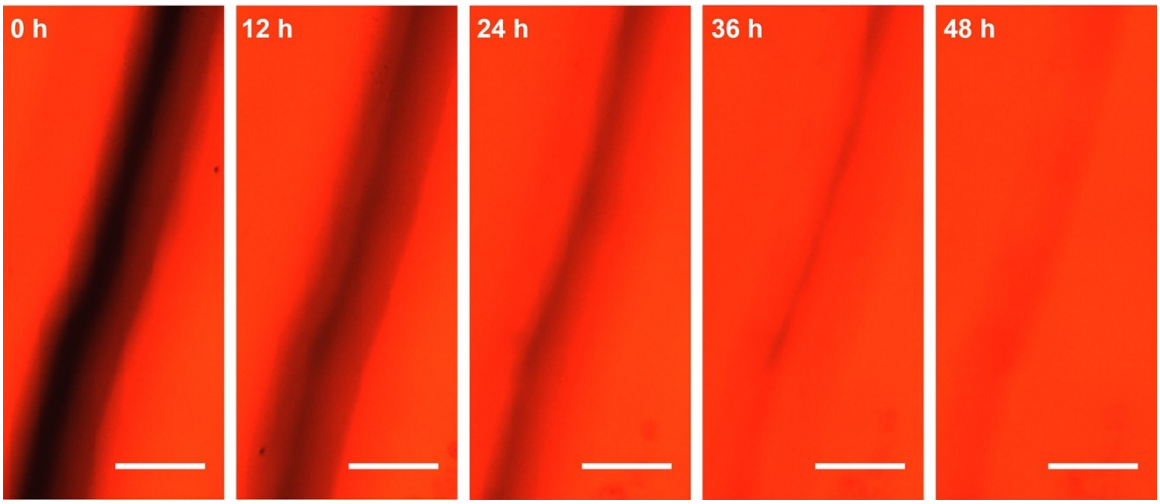

Figure S5. The time-resolved fluorescence microscope photographs of the autonomous self-healing of the polyionic elastomer. Scale bar: 50 μm.

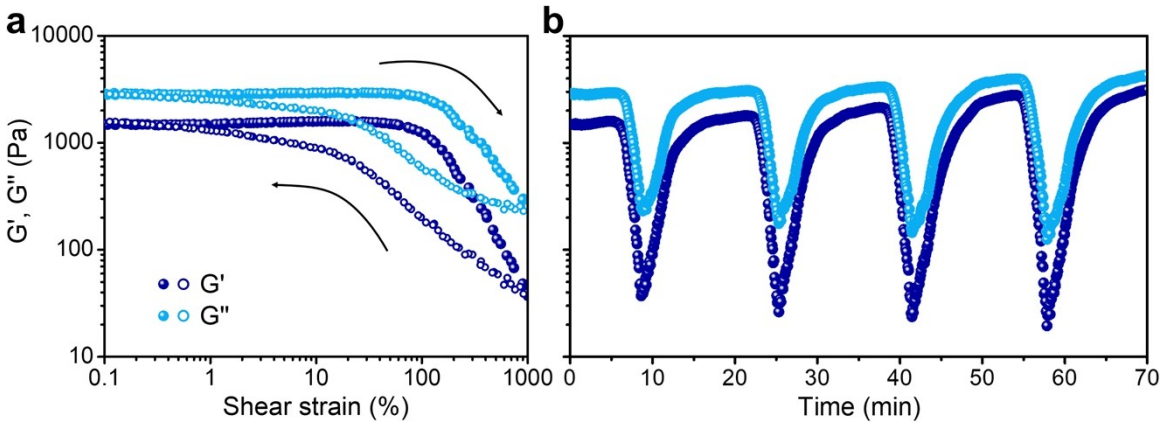

Figure S6. a, The oscillatory measurements (1 Hz) of the precursor ink, which sweep from 0.1% to 1000% and back to 0.1% strain. **b,** Cyclic oscillatory measurements from 0.1% to 1000% and back to 0.1% strain.

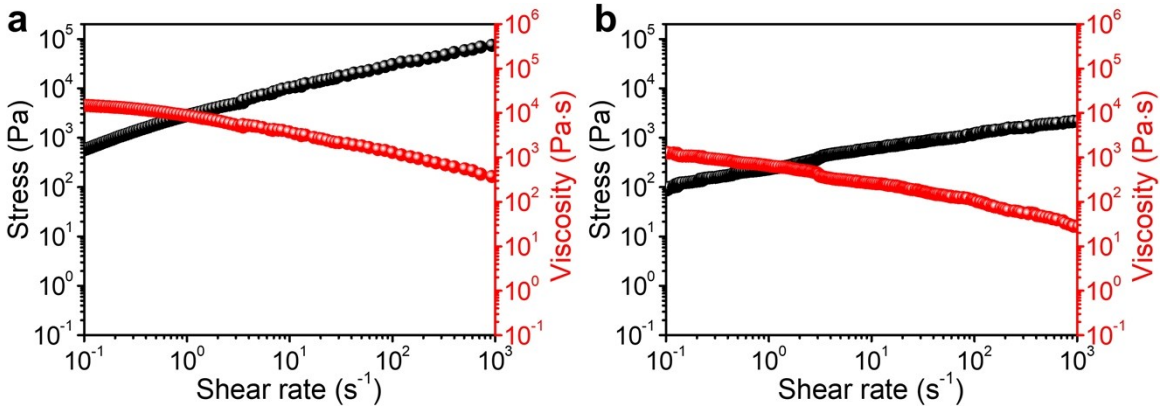

Figure S7. a, Shear-thinning behavior of the polyion precursor ink at 0 °C. **b,** Shear-thinning behavior of the polyion precursor ink at 50 °C.

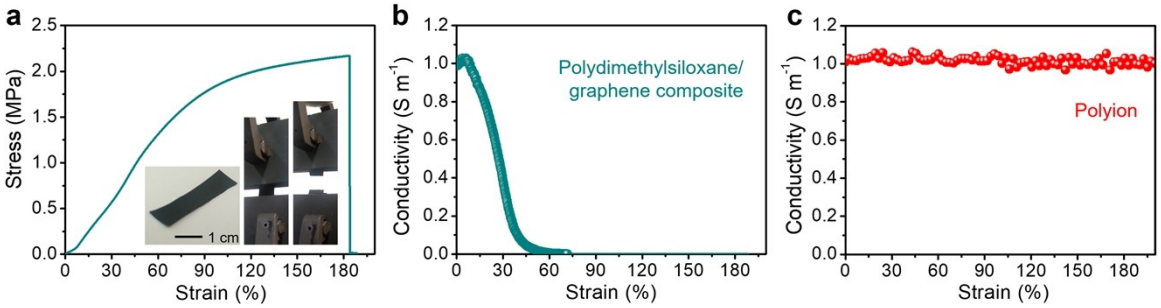

Figure S8. a, Tensile stress–strain curve of the polydimethylsiloxane/graphene composite at a strain rate of 0.013 s^{-1}. The inset pictures are a photograph of the electronic conductor and photographs of the composite before and after < 200% stretch. The maximum elongation at break is 184%. **b,** The conductivity degradation of the electronic conductor during stretch. The conductive networks totally break at 71% strain. **c,** In comparison, the conductivity of the polyionic elastomer is quite stable during stretch.

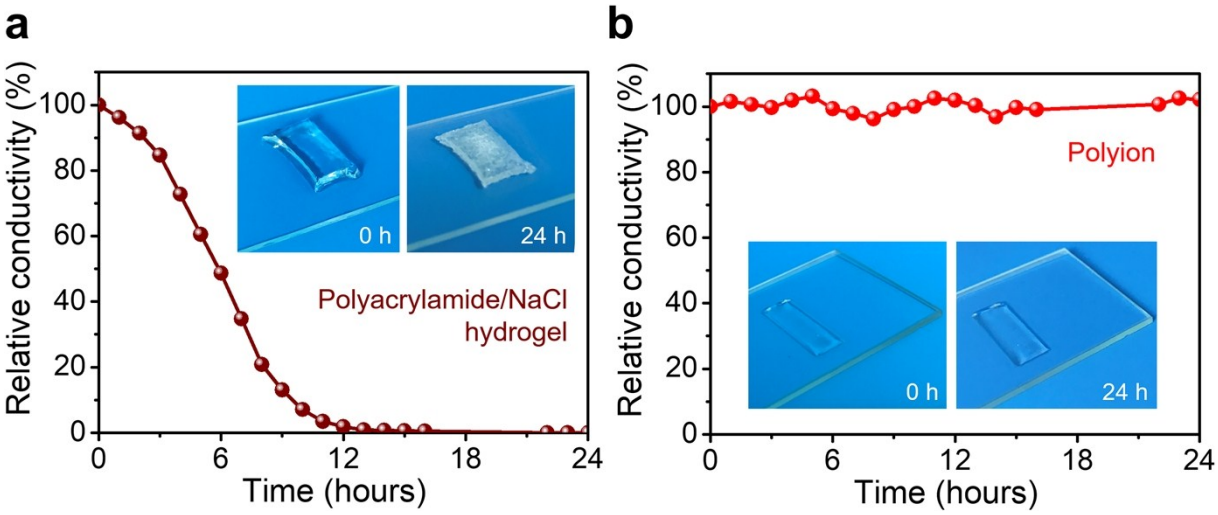

Figure S9. a, The relative conductivity change of a typical ionic conductor (a polyacrylamide/NaCl hydrogel) at ambient condition (25 °C, 60% RH). The inset pictures are the photographs of the hydrogel exposed to ambient atmosphere at 0 h and after 24 h. The decrease of the conductivity is ascribed to the loss of free water. **b,** In comparison, the polyionic elastomer is quite stable at ambient condition. The inset pictures are the photographs of the polyion exposed to ambient atmosphere at 0 h and after 24 h.

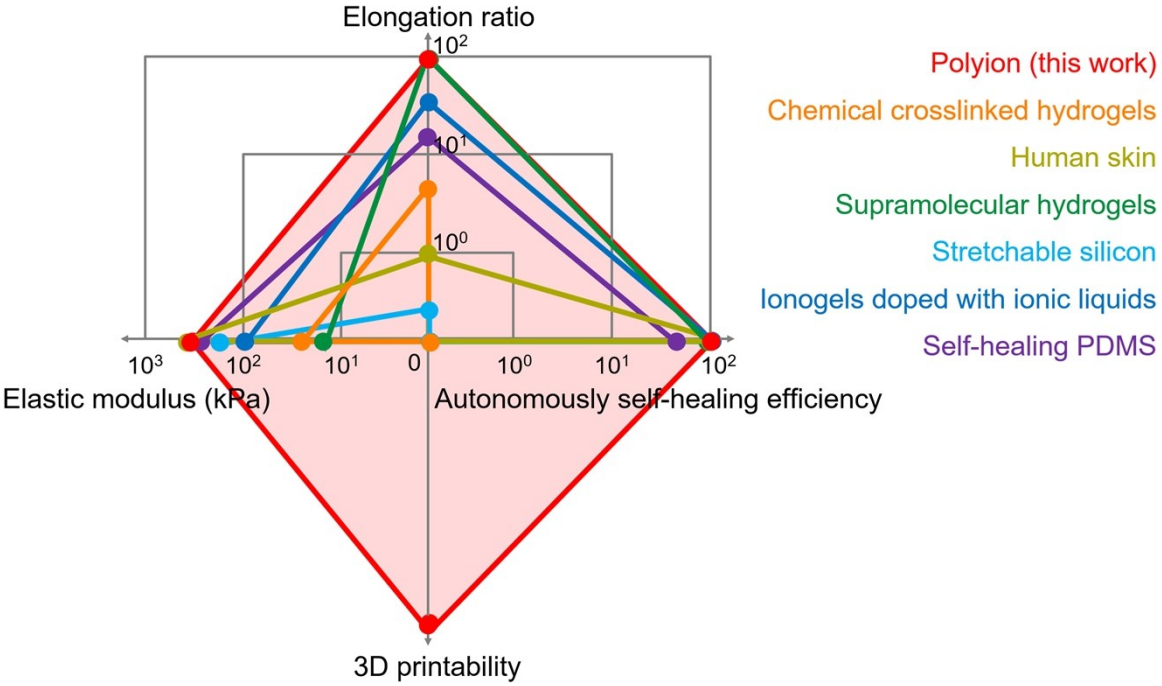

Figure S10. A comparison of mechanical properties among the polyionic elastomer, human skin and previously-reported skin-like materials.

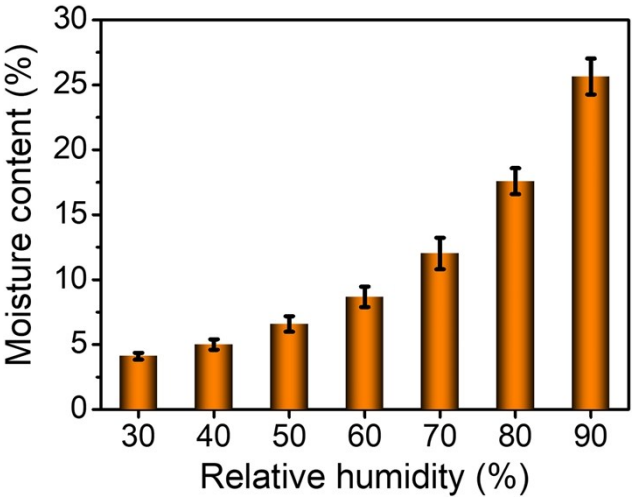

Figure S11. Moisture content of the polyionic elastomer at different RH.

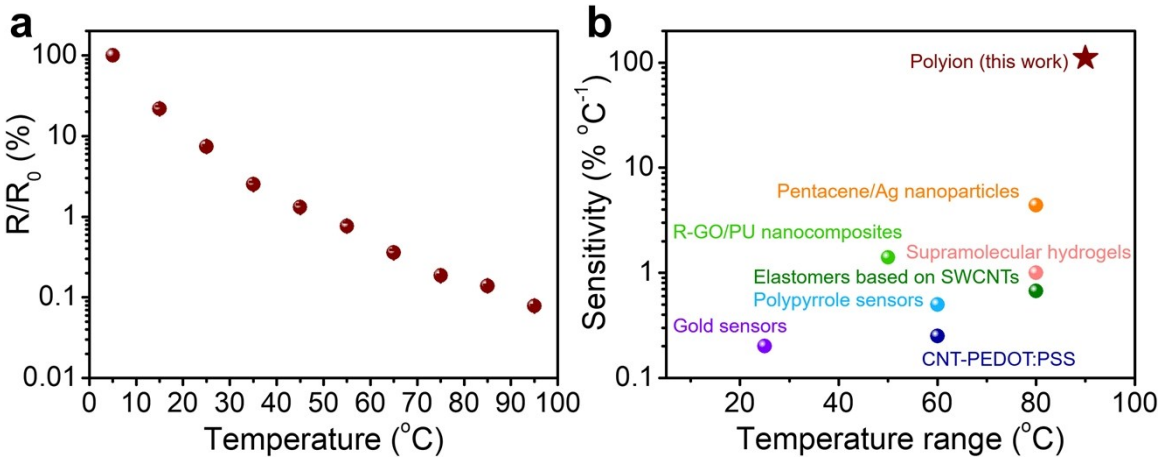

Figure S12. a, The resistance change of the polyionic elastomer in a wide temperature range from 5 to 95 °C at 60% RH. **b,** A comparison of thermal sensory capability between the polyionic elastomer and previously-reported skin-like thermal sensors.

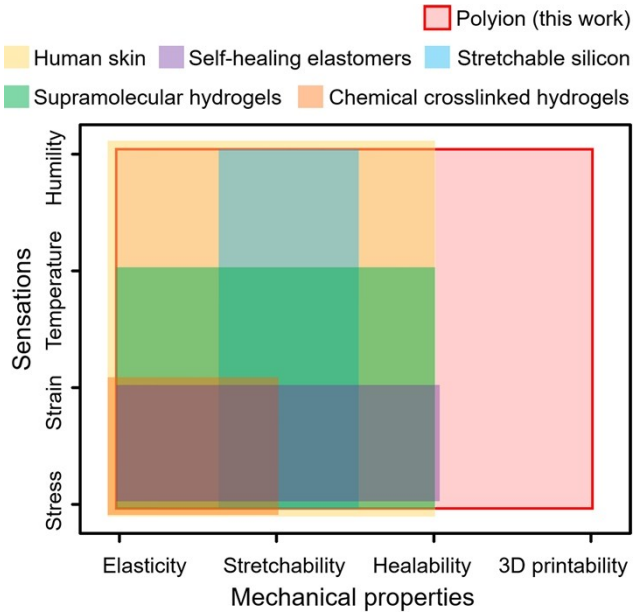

Figure S13. A comparison of mechanical properties and sensations among this work, human skin, and typical artificial skins based on self-healing elastomers[18, 19], stretchable silicon[20], supramolecular hydrogels[9], and chemical crosslinked hydrogels[2].

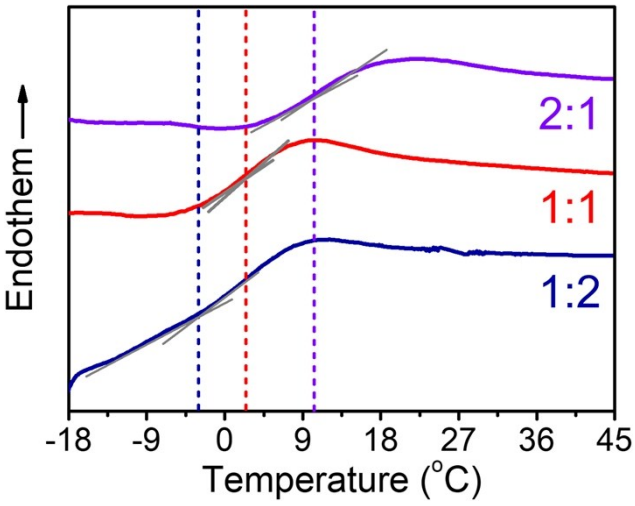

Figure S14. DSC curves of the polyionic elastomers. DSC curves of the polyionic elastomers with different counterion molar ratios show different glass transition temperatures (the molar ratio of anionic and cationic units varying from 1:2 to 2:1).

References

1. K. Tian, J. Bae, S. E. Bakarich, C. Yang, R. D. Gately, G. M. Spinks, M. in het Panhuis, Z. Suo and J. J. Vlassak, *Adv. Mater.*, 2017, **29**, 1604827.
2. J.-Y. Sun, C. Keplinger, G. M. Whitesides and Z. Suo, *Adv. Mater.*, 2014, **26**, 7608-7614.
3. D. P. J. Cotton, I. M. Graz and S. P. Lacour, *IEEE Sens. J.*, 2009, **9**, 2008-2009.
4. S. Yao and Y. Zhu, *Nanoscale*, 2014, **6**, 2345-2352.
5. C.-C. Kim, H.-H. Lee, K. H. Oh and J.-Y. Sun, *Science*, 2016, **353**, 682-687.
6. F. Zhao, H. Cheng, Z. Zhang, L. Jiang and L. Qu, *Adv. Mater.*, 2015, **27**, 4351-4357.
7. S. Zhang, K. H. Lee, C. D. Frisbie and T. P. Lodge, *Macromolecules*, 2011, **44**, 940-949.
8. A. J. D'Angelo and M. J. Panzer, *J. Phys. Chem. B*, 2017, **121**, 890-895.
9. Z. Lei and P. Wu, *Nature Commun.*, 2018, **9**, 1134.
10. R. K. Pandey, M. D. Hossain, S. Moriyama and M. Higuchi, *J. Mater. Chem. A*, 2014, **2**, 7754-7758.
11. R. C. Webb, A. P. Bonifas, A. Behnaz, Y. Zhang, K. J. Yu, H. Cheng, M. Shi, Z. Bian, Z.

Liu, Y.-S. Kim, W.-H. Yeo, J. S. Park, J. Song, Y. Li, Y. Huang, A. M. Gorbach and J. A. Rogers, *Nat. Mater.*, 2013, **12**, 938-944.

12. S. Harada, K. Kanao, Y. Yamamoto, T. Arie, S. Akita and K. Takei, *ACS Nano*, 2014, **8**, 12851-12857.
13. H. Yang, D. Qi, Z. Liu, B. K. Chandran, T. Wang, J. Yu and X. Chen, *Adv. Mater.*, 2016, **28**, 9175-9181.
14. Y. He, Q. Gui, S. Liao, H. Jia and Y. Wang, *Adv. Mater. Technol.*, 2016, **1**, 1600170.
15. T. Q. Trung, S. Ramasundaram, B.-U. Hwang and N.-E. Lee, *Adv. Mater.*, 2016, **28**, 502-509.
16. X. Ren, K. Pei, B. Peng, Z. Zhang, Z. Wang, X. Wang and P. K. L. Chan, *Adv. Mater.*, 2016, **28**, 4832-4838.
17. J. Jeon, H.-B.-R. Lee and Z. Bao, *Adv. Mater.*, 2013, **25**, 850-855.
18. B. C. K. Tee, C. Wang, R. Allen and Z. Bao, *Nature Nanotechnol.*, 2012, **7**, 825-832.
19. J. Kang, D. Son, G. J. N. Wang, Y. Liu, J. Lopez, Y. Kim, J. Y. Oh, T. Katsumata, J. Mun, Y. Lee, L. Jin, J. B. H. Tok and Z. Bao, *Adv. Mater.*, 2018, **30**, 1706846.
20. J. Kim, M. Lee, H. J. Shim, R. Ghaffari, H. R. Cho, D. Son, Y. H. Jung, M. Soh, C. Choi, S. Jung, K. Chu, D. Jeon, S.-T. Lee, J. H. Kim, S. H. Choi, T. Hyeon and D.-H. Kim, *Nature Commun.*, 2014, **5**, 5747.